ADDITIVE TECHNOLOGIES, POWDER AND COMPOSITE MATERIALS

FORMATION OF COMPOSITE MATERIAL BY MAGNETIC PULSE WELDING OF CRYSTALLINE TITANIUM AND NICKEL-BASED AMORPHOUS ALLOY

D. V. Lazurenko,[1] A. A. Ivannikov,[2] A. G. Anisimov,[3] N. S. Popov,[2] and G. D. Dovzhenko[4]

Three-layer composite materials composed of VT1-0 alloy plates and an amorphous layer of ST15 alloy between them, which were produced by magnetic pulse welding, have been studied. The structure of the composites was studied by scanning and transmission electron microscopy. The phase composition was determined using x-ray synchrotron radiation and electron diffraction. It is shown that the welding process causes partial remelting of the amorphous ribbon and its mixing with titanium, and the cooling causes re-amorphization. Titanium interacts with atmospheric gases and forms oxides and nitrides, which are distributed in the remelted zones of the amorphous layer in the form of particles not larger than 35 nm in size. Welding of the amorphous ribbon to the less active nickel does not produce additional phases.

Key words: magnetic pulse welding, dynamic interaction, diffraction of x-ray synchrotron radiation, metallic glass.

INTRODUCTION

Over the past decades, metallic glasses have attracted the attention of a large number of research groups due to the high potential of these materials. Metallic glasses have a unique set of mechanical and operation properties, among which high strength, corrosion and wear resistance can be distinguished. However, to date, they have not yet found wide application as structural materials. The main problems are related to the limited dimensions of blanks produced from metallic glasses and the low stability of their amorphous state.

One of the approaches to solving the problem of using metallic glasses is the formation of composite materials on their basis. Metallic glass powders are often used to reinforce metal matrix composites [1 – 3]. However, a number of studies are aimed at producing layered amorphous-crystalline materials [4, 5]. The main method of producing materials of this type is cold welding. These types of welding include impact welding, which in its turn can be explosion welding [6] and magnetic pulse welding [7]. Such methods are based on the same principle: high-speed collision of welded blanks [8]. Under these conditions, a cumulative jet is formed between the colliding blanks, which cleans the surfaces from oxides and contaminants. At the same time, high impact pressures cause deformation of metals within a short period of time. The surfaces to be welded, cleaned by the jet from oxides and contaminants, due to the action of very high pressures, are in close contact with each other and form an interatomic bond. Since the materials to be joined are heated only

[1] Novosibirsk State Technical University, Novosibirsk, Russia (e-mail: pavlyukova 87@mail.ru).

[2] National Research Nuclear University MEPhI, Moscow, Russia.

[3] Lavrent'evInstitute of Hydrodynamics of the Siberian Branch if the Russian Academy of Sciences, Novosibirsk, Russia.

[4] SKIF Common Access Centre, Boreskov Institute of Catalysis of the Siberian Branch of the Russian Academy of Sciences, Koltsovo, Russia.

in local areas concentrated in a thin boundary layer, it is possible to retain the amorphous state of metallic glass.

The results of studies of explosion welding of crystalline materials with amorphous foils can be found in certain literature sources. Thus, [9] presents a successful joining of bulk metallic glass (BMG) Ti40Zr25Cu12Ni3Be20 with aluminium. No signs of crystallization of the amorphous blank were found by the authors of [9]. Welding of aluminium with BMG of a slightly different composition (Zr60Ti17Cu12Ni11) was studied in [10, 11]; however, the joining was carried out by under water explosion welding. It has been established that the welding process was accompanied by the formation of an intermediate layer between amorphous plate and a crystalline plate, which had a crystalline structure. At that, the bulk of the metallic glass blank retained its amorphous state. Attempts to join a rapid-quenched nickel-based alloy with stainless steel by underwater explosion welding were made in [12, 13]. As a result, a high-quality joint was obtained while retaining the amorphous state of metallic glass. Articles [5, 14] are devoted to the joining of rapid-quenched alloys with copper, which has a high thermal conductivity and provides fast heat removal from the joining zone, which is an additional positive factor contributing to the retaining of the disordered structure of a rapid-quenched alloy.

Compared to explosion welding, magnetic pulse welding is less studied despite a number of its obvious advantages (including the possibility of wide industrial application, since it does not require the use of explosives and, in general, is a cleaner and more accurate method) [8]. Most of the studies devoted to magnetic pulse welding are concentrated on the research of joints of rod elements with flat ones [15, 16], tubular blanks [17], as well as moulding welding [18, 19]. A few studies of magnetic pulse welding of flat blanks are reduced to the research of joints of crystalline alloys [7, 20 – 23].

In our previous study, it was shown that magnetic pulse welding can be used to form amorphous-crystalline composite structures [24]. Titanium and titanium-based metallic glass were chosen as initial blanks in [24]. Studies of welds have shown that magnetic pulse welding can provide a high-quality joining of metal and amorphous blanks while retaining the disordered structure of metallic glass. It should be noted that in terms of the chemical composition, the materials in the welded pair can be called related (metallic glass contained approximately 50 wt.% of Ti). However, the question of joining materials with a radically different composition remains open.

The objective of this research is to study the influence of the compositions of metallic glass and crystalline alloy on the features of the formation of a welded joint during magnetic pulse welding.

METHODS OF STUDY

Titanium foils 170 μm thick and an amorphous ribbon made of ST15 alloy 65 μm thick were used as objects of study. The studied materials had the following chemical composition, wt.%: VT1-0 alloy — 99.33 Ti, 0.25 Fe, 0.07 C, 0.1 Si, 0.04 N, 0.2 O, 0.01 H; ST15 alloy — 68 Ni, 15 Cr, 7.5 Si, 4 Mo, 4 Fe, 1.5 B [25]. An amorphous ribbon was produced by the spinning method on a Kristall-702 unit [26]. The melt was cooled on a copper disk at its linear rotation speed of 20 m/sec in a helium atmosphere. The melt cooling rate was $10^4 – 10^6$ K/sec.

Magnetic pulse welding was carried out at the Lavrent'ev Institute of Hydrodynamics SB RAS [27]. The power source was a capacitor battery with a capacity of 3.4×10^{-3} F and a voltage of up to 5 kV. The inductance of the battery and input cables was within 40 nH. The battery discharge was initiated by a solid-state discharger. The capacitor battery accumulated up to 40 kJ of energy. The discharge current was recorded by an inductive sensor. In the course of the experiment, the magnetic pressure, the speed of the driver plate and its travel distance were assessed. This data was used to set the speed of impact between the driver and the fixed plates, changing the distance between them.

A plate made of copper 0.5 mm thick and 30 mm wide was used as a driver plate. The copper plate was not welded to the composite. The width of the welded ribbons was 20 mm. The blank length was 150 mm. The speed of the contact point and the angle of impact of the copper plate with the first titanium foil during welding were 1500 – 1800 m/sec and 13°, respectively.

To assess the influence of the crystalline material type on the features of the structure formation of the composite, a three-layer composite consisting of two plates of crystalline nickel (plate thickness of 170 μm) and an amorphous nickel-based alloy (65 μm thick) between them was additionally formed.

The structure of the produced composite was studied by scanning electron microscopy (SEM) using a Carl Zeiss EVO 50 microscope equipped with an Oxford Instruments X-Act energy dispersive x-ray microanalyzer. Samples for structural studies were prepared by grinding on sandpaper of various fineness (from 125 to 5 μm) and aluminium oxide powder with particle sizes from 5 to 1 μm and subsequent polishing using a colloidal solution of silicon oxide (0.04 μm).

To study the structure of crystalline phases, the method of backscattered electron diffraction (BSED) was used. Investigations were carried out using a Carl Zeiss Sigma 300 SEM equipped with an Oxford Instruments HKL Channel 5 detector. For BSED studies, the samples were ground using abrasive sand papers and aluminium oxide powder and polished with a colloidal solution of silicon oxide. At the final stage, the sample was polished with argon ions on a Technoorg Linda SEMPrep2 unit.
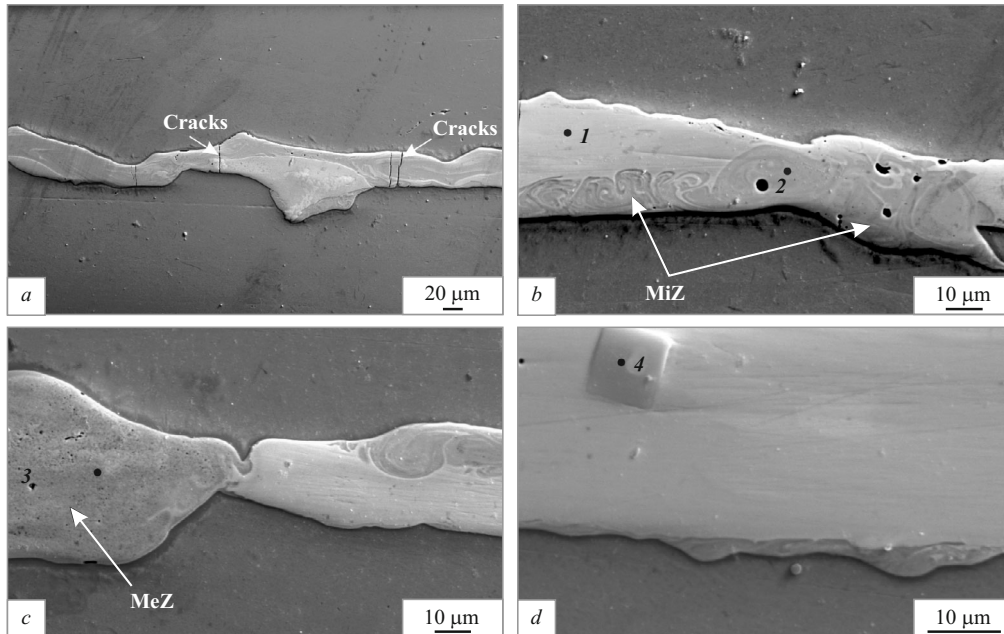
Fig. 1. Structure of various sections of the three-layer composite VT1-0 – ST15 – VT1-0 (cross section, SEM in the secondary electron mode): *a*) cracks in the amorphous layer; *b*) large pores; *c*) small pores; *d*) inclusion of a cubic form; *1*, *2*, *3*, *4* are the elemental analysis zones (see Table 1); MiZ is the mixing zone; MeZ is the melting zone.

The fine structure of the VT1-0-ST15 interface was studied by transmission electron microscopy (TEM) on a Carl Zeiss Libra 120 microscope. Foils for research were prepared by mechanical thinning of pre-cut plates on abrasive sand papers to a thickness of 100 μm and subsequent grinding of wells using a Gatan Dimple Grinder 656 sample preparation system. Final thinning was performed by an ion beam on a Gatan PIPS 659 unit.

Diffraction studies of the rapid-quenched foil were carried out on an ARL X'TRA laboratory diffractometer using a tube with a molybdenum anode. The survey was performed with a step of $2\theta = 0.02°$ and an accumulation time of 5 sec per point. The phase composition of the material after magnetic pulse welding was determined by x-ray synchrotron radiation diffraction. The measurements were carried out using a microbeam (130×130 μm^2) at the micro- and nanofocus x-ray scattering station (P03 The Micro- and Nanofocus x-ray Scattering, MiNaXS) of the German electronic synchrotron (Deutsches Elektronen-Synchrotron, DESY, Hamburg, Germany) in the "through light" mode. The cross section of the sample was preliminarily mechanically thinned to a thickness of 50 μm. The beam was centred on the ST15 alloy layer. Thus, the entire width of the amorphous ribbon and partly titanium layers fell into the survey area. The x-ray energy was 16.8 keV, which corresponded to a wavelength of about 0.738 Å. To record diffraction patterns, an EIGER 9M detector with a pixel size of 75×75 μm^2 was used. The distance from the sample to the detector was 253 mm. For calibration, lanthanum hexaboride powder was used. Azimuthal integration was performed using the PyFAI library for the Python programming language. The phase composition and cell parameters were determined using the PDF-4+ database and MAUD software [28].

RESULTS AND DISCUSSION

Three-layer composites containing two titanium layers and a layer of ST15 alloy between them were produced by magnetic pulse welding. Structural studies carried out by the SEM method indicate a reliable joint of the layers (Fig. 1*a*). The main processes that occur in the material under the conditions of impact welding are local deformation and heating, the signs of which are clearly observed in the microphotographs of the cross section. The deformation of the ST15 ribbon is evidenced by the uneven layer thickness over the section. The amorphous ribbon thickness in some areas was reduced to 10 μm.

Intense heating of separate sections caused their melting, which is confirmed by the formation of many small (Fig. 1*c*) and large (Fig. 1*b*) pores in local zones. The evidence that the ST15 material is in a liquid or extremely plastic state are the signs of turbulent flow in the zones bordering the crystalline layer. The presence of a visible contrast in the images of vortex formations indicates mixing of the materials to be welded in these zones.

The results of numerous theoretical and experimental studies testify to the intense heating of the mixing zones. The increase in temperature in these zones is facilitated by the
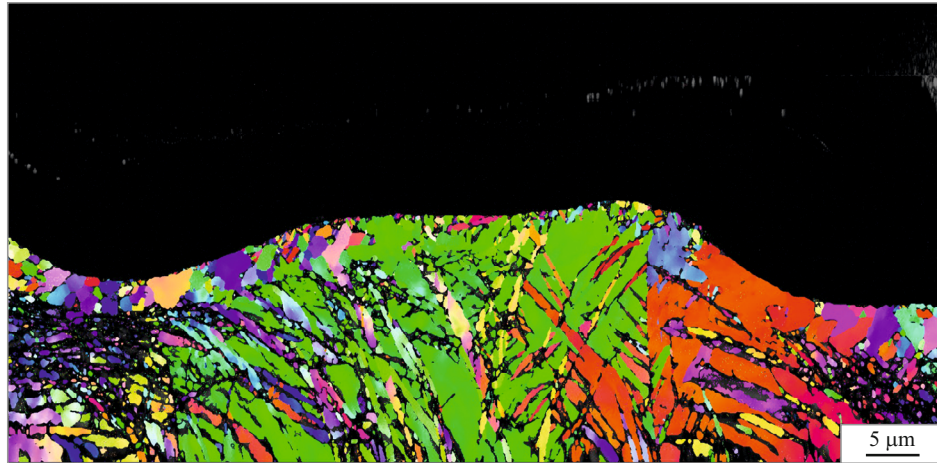
Fig. 2. Crystal orientation map, combined with the map illustrating the distribution of Kiku-chi-patterns by contrast. The image was obtained by the BSED method from the interface be-tween titanium and amorphous alloy.

heat released during plastic deformation near the impact point. Depending on the impact modes, the temperature of the zones can reach the melting temperature of the plates being welded. According to the assessment of the authors of [21] on the basis of simulation by the method of smoothed particle hydrodynamics, the heating temperature during magnetic pulse welding of iron with aluminium reached 1200 K, while the simulation of explosion welding gives much higher values [29].

An x-ray microspectral analysis of a zone with a lighter contrast showed that its elemental composition almost completely corresponds to the initial composition of the amorphous ribbon (see Table 1, spectrum *1*). Titanium was detected in the zone characterized by the generation of vortex formations, which is evidence of mixing of the surface layers of the blanks to be welded (see Table 1, spectrum *2*). In the remelting zone, the titanium content turned out to be even higher than that in the mixing zone (see Table 1, spectrum *3*). Thus, one can conclude that the composition of the amorphous ribbon has undergone local changes.

Other structural features revealed in the study of composites are cracks (Fig. 1*a*) and cubic inclusions (Fig. 1*d*) in the amorphous layer. Since the cracks are concentrated

mainly in the zones where the processes of welded materials mixing took place, one can conclude that their formation occurred at the stage of samples cooling after welding. The inclusions are probably defects in the amorphous ribbon formed during its manufacture, as evidenced by their location. Being outside the zones of remelting and vortex formation, they are characterized by an increased concentration of individual elements that make up the ST15 alloy. In particular, the inclusion shown in Fig. 1*d* contains an increased amount of chromium and molybdenum and practically does not have titanium (see Table 1, spectrum *4*).

In the context of the noted structural features, the question arises whether the ST15 alloy retained its amorphous state? Diffraction methods were used to determine the structure of the rapid-quenched layer. Figure 2 shows an image of one of the interfaces between ST15 and VT1-0, obtained by the BSED method. On the crystal orientation map, combined with the map illustrating the distribution of Kikuchi patterns by contrast, one can see that most of the sample is dark. It indicates the absence of Kikuchi lines, which is typical for amorphous materials. At the same time, small bright spots corresponding to fine crystallites can be observed in the amorphous layer. Thus, one can make a preliminary conclusion that the amorphous structure was partially preserved in the ST15 layer.

A number of structural features of the titanium alloy can also be observed in the image obtained by the BSED method. Near the interface between titanium and ST15 alloy, small grains were observed, the formation of which can be caused by one of the following factors. In the initial state, titanium had a coarse-grained structure. Upon impact, the welded plates were subjected to high-speed deformation. Near the interface, the deformation reaches its highest values, and the heat released in this case contributes to the recrystallization of the material in the boundary layers [29]. However, under conditions of high-speed impact, primary crystallization is

TABLE 1. Results of Energy Dispersive Analysis of Separate Zones of VT1-0 – ST15 – VT1-0 Composite

Spectrum (zone)*	Content of elements, wt.%					
	Ni	Cr	Si	Fe	Mo	Ti
1	67.6	15.1	9.2	4.1	3.6	0.4
2	46.5	10.3	5.8	2.9	2.7	31.8
3	38.5	8.5	4.7	2.4	2.3	43.6
4	6.7	46.2	—	1.9	44.7	0.5

* See Fig. 1.

also possible if the local zones are heated to the titanium melting temperature.

Confirmation of the retaining of the amorphous structure of the ST15 alloy are the results of analysis carried out by the x-ray diffraction method. Figure 3 shows an x-ray pattern obtained from a sample of a rapid-quenched alloy in its initial state. A typical diffuse halo is seen, indicating a disordered structure of the material. In addition to the halo, the x-ray diffraction pattern shows two diffraction peaks corresponding to nickel, which is the main component of this alloy. Thus, the initialST15 alloy contained a fraction of the crystalline phase.

The diffraction pattern obtained from the cross section of the composite material produced by magnetic pulse welding also contains a halo, indicating the retaining of the amorphous structure in the ST15 layer. In addition to the halo, reflections from nickel are visible. The x-ray diffraction pattern also shows α-Ti reflections obtained from titanium plates and additional peaks. X-ray structural analysis showed that these peaks correspond to a compound having an fcc lattice (PGSFm$\bar{3}$m) with a cell period $a = 4.24$ Å. Since the composition of the amorphous ribbon is quite complex, it is not possible to uniquely identify this phase. However, titanium oxides and nitrides can have such a crystal structure and cell period. In addition, the x-ray diffraction pattern shows an additional peak at $q = 3.21$ Å^{-1} (q is the scattering vector, defined as $q = \dfrac{4\pi}{\lambda}\sin\theta$), which, most likely, was obtained as a result of diffraction by an individual particle released in a rapid-quenched alloy during its production (Fig. 1d).

The TEM and electron diffraction methods were used to study the features of the crystalline phase distribution in the sample. Figure 4a shows the interface between titanium and an ST15 amorphous ribbon. The rapid-quenched layer, located in the interface zone with the titanium alloy, contained a large number of small particles up to 35 nm in size (Fig. 4b). With distance from the interface, the content of nano-releases in the amorphous layer decreased (Fig. 4c). The diffraction pattern (Fig. 4d) obtained from the zone shown in Fig. 4c contains both diffraction rings and an amorphous halo, which indicates the presence of a crystalline and disordered structures in this zone. It is shown that the diffraction rings in this electron diffraction pattern correspond to the fcc phase, which was detected in the analysis of the x-ray diffraction pattern obtained by x-ray synchrotron radiation diffraction (Fig. 3).

Due to the fact that the highest temperatures and local material melting are achieved near the impact point, the molten metal has the possibility of direct contact with the air atmosphere. Given the extremely high reactivity of molten titanium, the formation of oxides and nitrides in the mixing zones is quite justified. The formation of oxides and nitrides is also evidenced by the fact that as the distance from the interaction zone of the welded plates increases, the amount of
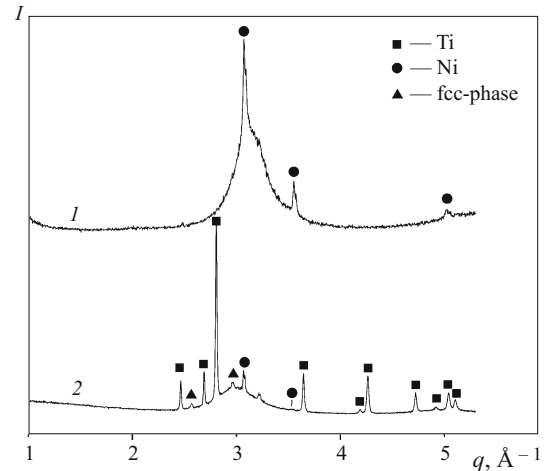

Fig. 3. X-ray pattern of the rapid-quenched ST15alloy (*1*) and the three-layer VT1-0 – ST15 – VT1-0 composite (*2*) produced by magnetic pulse welding.

nano-releases decreases, since the most active interaction with atmospheric gases occurs in the surface layers. In our previous research on the study of the interaction of VT1-0 titanium with a titanium-based amorphous alloy, it was shown [24] that crystalline titanium was released in the mixing zones. At that, the fcc phase was reliably identified only by x-ray synchrotron radiation diffraction. Analysis of the electron diffraction patterns did not reveal the presence of oxides and nitrides, which kept questions about the distribution of these phases in the sample. However, it is likely that the fcc phase was not previously detected by electron diffraction method due to the close location in the electron diffraction pattern of reflections from the (111) and (01$\bar{1}$0), (200) and (1$\bar{1}$01), (220) and (11$\bar{2}$0) planes of the fcc phase and α-Ti, respectively.

Release of additional phases in the amorphous layer was not detected; despite heating in the mixing zones to temperatures exceeding the temperature of crystallization and even melting of the amorphous alloy, its complete devitrification did not occur. The amorphous state was also not affected by the introduction of additional titanium into the local zones of the welds due to the mixing of the surface layers of the materials being welded. The results of the analysis performed by the x-ray diffraction method indicate a certain shift of the amorphous halo towards smaller angles on the x-ray diffraction pattern of the material after magnetic pulse welding. It is known that the halo position on the x-ray pattern at 2θ, as a rule, corresponds to the most intense peak of the crystalline element, which is predominant in the amorphous alloy composition. In this regard, the shift of the halo towards the location of the most intense titanium peak indicates a shift in the elemental composition of the rapid-quenched material. Thus, despite dilution with titanium, the ST15 alloy underwent re-amorphization in the magnetic pulse welding process. This phenomenon is associated with high cooling rates of the
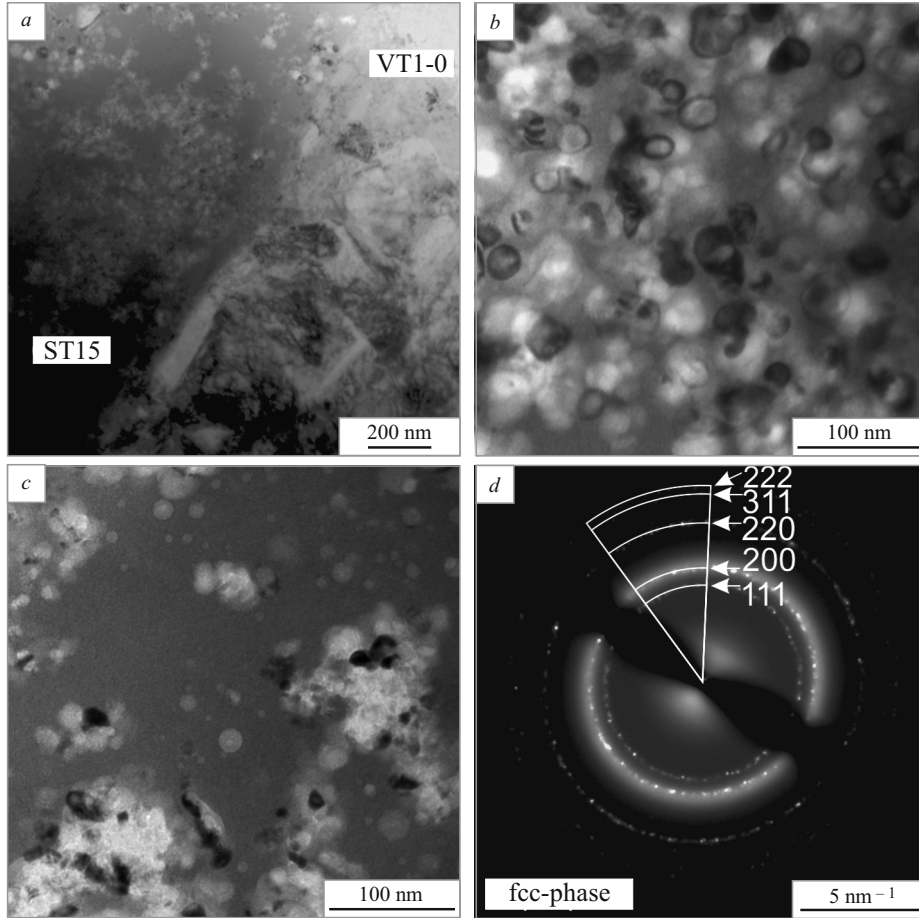
Fig. 4. Structure of various zones of the VT1-0 – ST15 – VT1-0 composite: *a*) at the interface between the VT1-0 and ST15 layers; *b*, *c*) ST15 alloy near the interface with titanium and at some distance from the interface with titanium, respectively; *d*) electron diffraction pattern obtained from the zone in Fig. 4*c*.

mixing zones formed during impact welding, which can reach $10^6 – 10^7$ K/sec, which is comparable with the rates required for the formation of an amorphous alloy [30]. Such
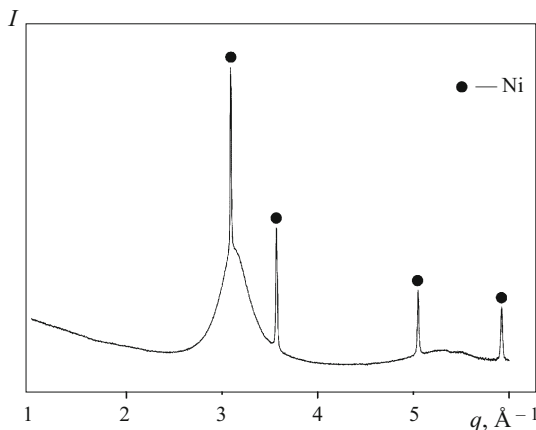

Fig. 5. X-ray diffraction pattern of the three-layer Ni – ST15 – Ni composite produced by magnetic pulse welding.

high cooling rates can cause not only repeated glass transition of alloys prone to amorphization, but also lead to amorphization of materials that were initially in the crystalline state [21, 22].

Based on the results obtained, several conclusions can be drawn. Excessive heat and mixing of welded crystalline and amorphous materials does not lead to devitrification of the amorphous alloy. Thus, in terms of retaining the disordered structure of the amorphous alloy, the requirements for welding modes can be minimal. The selection of modes should be primarily aimed at ensuring the formation of a high-quality welded joint. At that, restrictions are imposed by the interaction of active metals (in particular, titanium) with atmospheric gases in a heated and molten state. To confirm this conclusion, Fig. 5 shows an x-ray diffraction pattern of a composite material produced by magnetic pulse welding of a nickel-based amorphous ribbon with crystalline nickel under the same conditions. Less reactive compared to titanium, nickel did not form oxides or other phases with atmospheric gases during welding, as evidenced by the absence of any reflections in the diffraction pattern, except for nickel ones.

CONCLUSIONS

Three-layer VT1-0 – ST15 – VT1-0 composite materials containing crystalline titanium and an amorphous phase interlayer were produced by magnetic pulse welding. In the welding process, the local zones of the materials to be joined were subjected to intense high-speed deformation and heating to the melting temperature of the rapid-quenched alloy. In a titanium thin layer adjoining the interface with an amorphous alloy, a fine-grained structure, which appeared as a result of recrystallization processes or primary crystallization, was observed. In the zones subjected to maximum heating and deformation, mixing of the welded materials occurred, as evidenced by the presence of titanium in their composition. Despite the change in the ST15 alloy composition due to dilution with titanium, the high rates of heat removal from these zones contributed to its re-amorphization. Titanium, which is characterized by high reactivity, interacted with atmospheric gases, which led to the formation of oxides and nitrides distributed in the form of nano-inclusions in an amorphous matrix. When welding a less active metal (nickel) with an amorphous alloy, the formation of oxides and nitrides was not detected.

REFERENCES

1. V. I. Kvashnin, D. V. Dudina, A. V Ukhina, et al., "The benefit of the glassy state of reinforcing particles for the densification of aluminum matrix composites," *J. Compos. Sci.*, **6**(5), 135 (2022).
2. S. Scudino, K. B. Surreddi, S. Sager, et al., "Production and mechanical properties of metallic glass-reinforced Al-based metal matrix composites," *J. Mater. Sci.*, **43**, 4518 – 4526 (2008).
3. A. Samanta, H. J. Fecht, I. Manna, and P. P. Chattopadhyay, "Development of amorphous phase dispersed Al-rich composites by rolling of mechanically alloyed amorphous Al – Ni – Ti powders with pure Al," *Mater. Chem. Phys.*, **104**(2 – 3), 434 – 438 (2007).
4. W. D. Liu, K. X. Liu, Q. Y. Chen, et al., "Metallic glass coating on metals plate by adjusted explosive welding technique," *Appl. Surf. Sci.*, **255**(23), 9343 – 9347 (2009).
5. A. Chiba, Y. Kawamura, M. Nishida, and T. Yamamuro, "Explosive welding of ZrTiCuNiBe bulk metallic glass to crystalline Cu plate," *Mater. Sci. Forum*, **673**, 119 – 124 (2011).
6. I. D. Zakharenko, *Explosion Welding of Metals* [in Russian], Nauka i Tekhnika, Minsk (1990).
7. M. N. Kazeev, V. S. Koidan, V. F. Kozlov, and Yu. S. Tolstov, "Investigation of magnetic pulse welding in plane geometry," *Prikl. Mekh. Tekhn. Fiz.*, **54**[6(332)], 38 – 44 (2013).
8. A. Kapil and A. Sharma, "Magnetic pulse welding: An efficient and environmentally friendly multi-material joining technique," *J. Clean. Prod.*, **100**, 35 – 58 (2015).
9. K. X. Liu, W. D. Liu, J. T. Wang, et al., "Atomic-scale bonding of bulk metallic glass to crystalline aluminum," *Appl. Phys. Lett.*, **93**(8), 081918 (2008).
10. L. Hanliang, L. Ning, L. Xiaojie, et al., "Joining of Zr60Ti17Cu12Ni11 bulk metallic glass and aluminum 1060 by underwater explosive welding method," *J. Manuf. Process.*, **45**, 115 – 122 (2019).
11. H. Liang, N. Luo, T. Shen, et al., "Experimental and numerical simulation study of Zr-based BMG/Al composites manufactured by underwater explosive welding," *J. Mater. Res. Technol.*, **9**(2), 1539 – 1548 (2020).
12. K. Hokamoto, K. Nakata, A. Mori, et al., "Microstructural characterization of explosively welded rapidly solidified foil and stainless steel plate through the acceleration employing underwater shock wave," *J. Alloy. Compd.*, **485**(1 – 2), 817 – 821 (2009).
13. K. Hokamoto, K. Nakata, A. Mori, et al., "Dissimilar material welding of rapidly solidified foil and stainless steel plate using underwater explosive welding technique," *J. Alloy. Compd.*, **472**(1 – 2), 507 – 511 (2009).
14. J. Feng, P. Chen, and Q. Zhou, "Investigation on explosive welding of Zr53Cu35Al12 bulk metallic glass with crystalline copper," *J. Mater. Eng. Perform.*, **27**(6), 2932 – 2937 (2018).
15. S. V. Neskoromnyi, "The research of condenser welding of rod components with flat base," *Vestn. Donsk. Gos. Tekh. Univ.*, **9**(S1), 70 – 77 (2009).
16. E. L. Strizhakov, R. V. Merkulov, and N. E. Strizhakova, "Analysis of high-voltage pulsed welding with magneticpulse drive," *Potents. Sovr. Nauki*, No. 3(11), 58 – 62 (2015).
17. M. A. Poleshchuk, I. V. Matveev, and V. A. Bovkun, "Fields of application of magnetic pulse welding (review)," *Avtomat. Svarka*, No. 4(706), 47 – 52 (2012).
18. S. V. Neskoromnyi and E. L. Strizhakov, "Technology for producing stamp-welded lightweight housings for terminating an electric cable," *Vektor Nauki Tol'yat. Gos. Univ.*, No. 2-2(32-2), 123 – 129 (2015).
19. E. L. Strizhakov, N. A. Karandashev, V. V. Plotnikov, et al., "Magnetic pulse stamping-welding of shell structures," *Kuzn.-Shtamp. Proizvod., Obrab. Mater. Davlen.*, No. 3, 12 – 14 (2002).
20. M. Watanabe and S. Kumai, "Dissimilar metal lap welding of A5052 aluminum alloy and TP340 pure titanium plates by using magnetic pulse welding," *J. Light Met. Weld.*, **58**, 91 – 96 (2020).
21. H. Geng, J. Mao, X. Zhang, et al., "Formation mechanism of transition zone and amorphous structure in magnetic pulse welded Al – Fe joint," *Mater. Lett.*, **245**, 151 – 154 (2019).
22. H. Yu, H. Dang, and Y. Qiu, "Interfacial microstructure of stainless steel/aluminum alloy tube lap joints fabricated via magnetic pulse welding," *J. Mater. Process. Technol.*, **250**, 297 – 303 (2017).
23. J. Cui, L. Ye, C. Zhu, et al., "Mechanical and microstructure investigations on magnetic pulse welded dissimilar AA3003-TC4 joints," *J. Mater. Eng. Perform.*, **29**(1), 712 – 722 (2020).
24. D. V. Lazurenko, A. G. Anisimov, N. S. Popov, et al., "Joining Ti-based metallic glass and crystalline titanium by magnetic pulse welding," *J. Non-Cryst. Solids*, **597**, Art. 121912 (2022).

25. M. A. Penyaz, N. S. Popov, A. A. Ivannikov, and O. N. Sevryukov, "Alloying-dependent microstructure influence on corrosion resistance of AISI 321 cell joints brazed by Ni-based filler metals," *Non-Ferrous Met*., **48**(1), 41 – 48 (2020).

26. B. A. Kalin, V. T. Fedotov, O. N. Sevryukov, and A. E. Grigor'ev, "Amorphous strip brazing alloys for high-temperature brazing. Experience with developing production technology and application," *Weld. Int*., **10**(7), 578 – 581 (1996).

27. A. G. Anisimov and V. I. Mali, "Peculiarities of driver plate under magnetic pulse welding," *Fiz. Goren. Vzryva*, **54**(1), 125 – 131 (2018).

28. L. Lutterotti, S. Matthies, and H. R. Wenk, "MAUD: a friendly Java program for material analysis using diffraction," *CPD Newslett*., **21**, 14 – 15 (1999).

29. I. A. Bataev, S. Tanaka, Q. Zhou, et al., "Towards better understanding of explosive welding by combination of numerical simulation and experimental study," *Mater. Design*, **169**, 107649 (2019).

30. I. A. Bataev, "Structure of explosivelywelded materials: experimental study and numerical simulation," *Obrab. Metal. (Tekhnol. Oborud. Instrum.)*, **4**(77), 55 – 67 (2017).